Solar Energy Materials & Solar Cells 140 (2015) 275–280

Contents lists available at ScienceDirect

Solar Energy Materials & Solar Cells

journal homepage: www.elsevier.com/locate/solmat

Application and modeling of an integrated amorphous silicon tandem based device for solar water splitting

Félix Urbain [a,*], Vladimir Smirnov [a], Jan-Philipp Becker [a], Uwe Rau [a], Jürgen Ziegler [b], Bernhard Kaiser [b], Wolfram Jaegermann [b], Friedhelm Finger [a]

[a] IEK-5 Photovoltaik, Forschungszentrum Jülich, D-52425 Jülich, Germany
[b] Institute of Materials Science, TU Darmstadt, D-64287 Darmstadt, Germany

ARTICLE INFO

Article history:
Received 29 October 2014
Accepted 7 April 2015

Keywords:
Water splitting
Hydrogen production
Silicon
Photoelectrochemical cell
Photocathode

ABSTRACT

Direct solar-to-hydrogen conversion via water splitting was demonstrated in an integrated photovoltaic–electrochemical (PV–EC) device using a hydrogenated amorphous silicon thin film tandem junction (a-Si:H/a-Si:H) solar cell as photocathode. The solar cell was adapted to provide sufficient photovoltage to drive both the hydrogen and oxygen evolution reactions. The best results, in terms of photoelectrochemical stability and performance, were obtained with an Ag/Pt layer stack as H_2 evolving photocathode back contact and with a RuO_2 counter electrode for O_2 evolution. Under irradiation by simulated sunlight (AM 1.5 spectrum with 100 mW/cm^2), we achieved 6.8% solar-to-hydrogen efficiency at 0 V applied bias in a two-electrode set-up. This sets a fresh benchmark for integrated thin film silicon tandem based photoelectrochemical devices. In addition, the photovoltage at constant current (-3 mA/cm^2) was measured over a prolonged period of time and revealed an excellent chemical stability (operation over 50 h) of the photocathode. Furthermore, we present an empirical serial circuit model of the PV–EC device, in which the corresponding photovoltaic and electrochemical components are decoupled. This allows for a detailed comparison between the solar cell and the PV–EC cell characteristics, from which the relevant loss processes in the overall system could be identified. The model was further used to compare calculated and measured photocurrent–voltage characteristics of the investigated PV–EC device which showed excellent agreement.

1. Introduction

Solar-driven hydrogen production via water splitting using sunlight as the only energy input holds great promise as a sustainable energy source which allows for the direct conversion and storage of energy in the form of a chemical bond, namely H_2. It addresses the need to produce storable fuels from fluctuating renewable energy sources and may pave the way for future commercial applications [1–3]. The technical and commercial viability, however, is closely linked to the efficiency and cost-effectiveness of such energy concepts. Integrated semiconductor based photoelectrochemical systems may provide adequate candidates and have recently been attracting considerable interest among research groups worldwide [4].

Electrochemical photolysis was first reported by Honda and Fujishima in 1972 using TiO_2 [5]. Since then, a variety of semiconducting materials and device configurations have been examined for their usability as photoelectrodes for solar water splitting [6,7]. The main requirement to the photoelectrodes is to generate a photovoltage well above 1.23 V, which is the minimum thermodynamic potential difference under standard conditions to produce H_2 and O_2 from water (disregarding overpotential losses, typically in the range of >0.4 V [8]) via the hydrogen evolution reaction (HER) and the oxygen evolution reaction (OER). Once a sufficiently high photovoltage is exceeded, the efficiency of the process is determined by the photocurrent density provided by the photoelectrode. Furthermore, the electrode has to be stable under the rough conditions present during gas evolution in aqueous electrolytes or it has to be covered by a protective coating [9]. Examples for investigated photocathodes are III–V semiconductors (e.g. InP [10], GaP [11], GaInP2 [12]), crystalline Si [13–15], V–I dichalcogenides [16–19] and $CuIn_xGa_{1-x}Se_2$ [20]. Candidates for photoanode materials are mainly metal oxides (e.g. Fe_2O_3 [21], WO_3 [22], and $BiVO_4$ [23]) due to their stability under oxidizing conditions. Wide band gap single junction absorber materials may provide enough photovoltage, but suffer from low photocurrents, and therefore exhibit low efficiencies. In contrast, photovoltaic (PV) based tandem structures which combine two solar cells in

* Corresponding author. Tel.: +49 2461 613242.
E-mail address: f.urbain@fz-juelich.de (F. Urbain).

http://dx.doi.org/10.1016/j.solmat.2015.04.013

series, hold great promise for direct applications in photoelectrochemical water splitting devices. Tandem structures can generate a photovoltage large enough to operate a photoelectrochemical cell (PEC) system without an external bias and allow for a more efficient utilization of the solar spectrum and hence the generation of higher photocurrents [24–26].

To date, standalone solar water-splitting systems have only been reported for III–V semiconductors [12,27], triple junction solar cells [28], or for PEC systems, which use tandem structures as additional bias for a photoactive metal oxide anode [23,29,30]. The widespread use, in particular of III–V semiconductor structures, is however still hampered by stability issues and cost limitations. In this regard, silicon based thin film technology, which stands out due to its chemical resistance, earth abundance and low cost production [13,31] may present a promising pathway to sustainable solar hydrogen production. Therefore, the main focus of this study is the implementation and characterization of a high photovoltage (V_{OC}=1.87 V) amorphous silicon tandem junction solar cell as photocathode in a PV–EC device, in terms of chemical stability and performance. Moreover, to elucidate the overall behavior of the PV–EC device, a detailed loss analysis was performed based on an empirical serial circuit model. This will allow to closely link the photovoltaic (PV) performance of the used solar cell with the photovoltaic–electrochemical (PV–EC) behavior of the integrated device.

2. Material and methods

The tandem junction photocathode, as shown in Fig. 1, was made in a p-i-n-p-i-n superstrate configuration and was deposited on 100 cm^2 fluorine-doped tin oxide (SnO_2:F) coated glass substrate (Asahi U). Both intrinsic a-Si:H sub cell absorber layers were deposited at a substrate temperature of 130 °C and a silane concentration of 4% from silane-hydrogen gas mixture using a plasma enhanced chemical vapor deposition (PECVD) process. Top and bottom cell had a thickness of 90 nm and 400 nm, respectively. Details on the preparation of thin silicon layers and solar cells can be found elsewhere [32]. Ag and Pt metal layers were deposited by means of electron beam evaporation at a thickness of approximately 700 nm and 50 nm, respectively. A 80 nm thick sputtered aluminum doped zinc oxide (ZnO:Al) layer between the silicon and the Ag layer helps in reducing optical losses in the device [33]. As depicted in Fig. 1, the metallic layer at the rear side functions as light-reflecting back contact and at the same time as electrocatalyst for the HER. In this regard, a double metal layer back contact structure of Ag and Pt was applied on the a-Si:H/a-Si:H photocathode. A 700 nm thick Ag layer was used to ensure a good reflectivity of the incoming light, and thus allow for a high photocurrent. A thin Pt layer (50 nm) was deposited on top of the Ag layer as a catalyst for the HER. The back contact additionally protects the ZnO:Al layer from the acidic electrolyte.

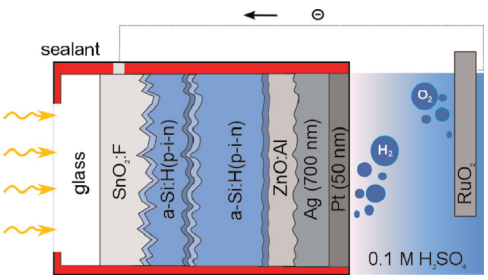

Fig. 1. Schematic drawing of the integrated PV–EC device under operation with the a-Si:H/a-Si:H photocathode and a RuO_2 anode. Hydrogen evolution occurs at the rear side of the a-Si:H/a-Si:H photocathode.

The solar cell was characterized by current–voltage (*J–V*) measurements under AM 1.5 illumination using a double source (Class A) sun simulator. The photoelectrochemical performance of the electrodes (photocathode and anode) was evaluated at room temperature in an aqueous 0.1 M sulfuric acid (H_2SO_4) electrolyte solution using three-electrode and two-electrode configurations [34]. The photocathode was illuminated with a sun simulator (Newport Oriel LCS-100) with AM 1.5 G filter (100 mW/cm^2). The set-up of the self-built electrochemical cell consisted of a Teflon cell body and two or three-electrodes, respectively: a working electrode (a-Si:H/a-Si:H photocathode, 8 mm diameter), a counter electrode, composed of a ruthenium oxide (RuO_2) coated titanium sheet (15 g/m^2 RuO_2, supplied by Metakem) and, for the three-electrode measurements, a Ag/AgCl reference electrode being in contact with 3 M sodium chloride (NaCl). The potential of the working electrode was controlled by a potentiostat (Metrohm, μAutolab Type III). The distance between the working and the counter electrode was about 20 mm. Electrical contact to the SnO_2:F coated substrate, i.e. the front contact of the photocathode, was made by a silver paste.

Under operation of the PV–EC device the electrons are injected from the rear side (Pt layer) of the photocathode into the electrolyte for the HER (see Fig. 1) and thus the holes are transferred from the TCO front contact (SnO_2:F) of the photocathode to the anode (RuO_2) for the OER. Both electrodes are separated through an electrolyte (0.1 M H_2SO_4). This configuration offers the advantage that the light enters the photocathode through the glass substrate without being attenuated by a surrounding medium (e.g. the electrolyte or gas bubbles).

3. Results and discussion

3.1. a-Si:H/a-Si:H photocathode

The photovoltaic performance of the investigated a-Si:H/a-Si:H tandem solar cell along with the photovoltaic parameters is shown in Fig. 2.

The tandem solar cell was developed with focus on high photovoltage in order to be suitable for water splitting [32]. The cell has an electrical conversion efficiency of 9.9% and provides a high V_{OC} of 1.87 V and a J_{SC} of 6.8 mA/cm^2. The PV–EC device operates most efficiently at the maximum power point of the corresponding solar cell, i.e. below 1.6 V (V_{mpp}). The water splitting reactions require a potential of 1.23 V. Hence, additional losses in the PV–EC system should not exceed 370 mV (1.6–1.23 V). A detailed analysis of the relevant loss processes will be discussed in Section 3.3.

For water splitting applications highly stable photoelectrodes are desirable. As can be seen in Fig. 1 the Pt contact is the only part of the photocathode that comes into contact with the electrolyte.

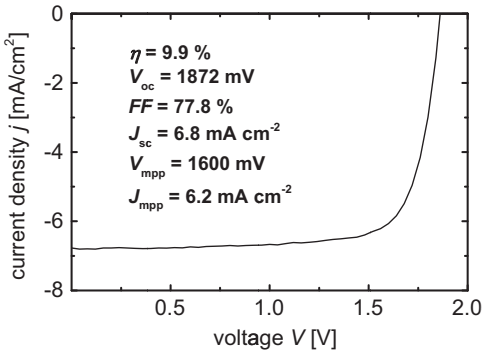

Fig. 2. Photocurrent–voltage measurement of the investigated a-Si:H/a-Si:H tandem junction solar cell with a ZnO:Al/Ag back reflector.

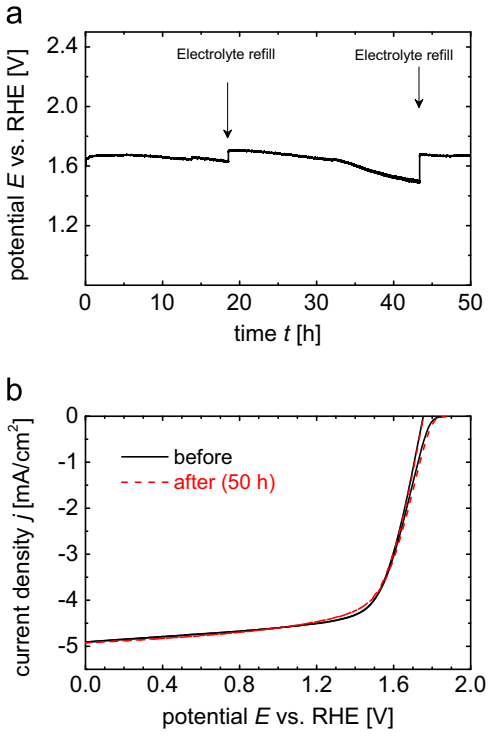

Fig. 3. (a) Chronopotentiometry measurement of the a-Si:H/a-Si:H photocathode with Ag/Pt contact at a constant photocurrent density of -3 mA/cm^2 in a three-electrode configuration. The measurements were conducted in a 0.1 M H_2SO_4 solution. The arrows indicate electrolyte refills. (b) Cyclic voltammetry measurement before (black solid curve) and after the 50 h stability test (red dotted curve) of the investigated photocathode. The measurements were conducted in a 0.1 M H_2SO_4 solution at a scan rate of 30 mV/s. (For interpretation of the references to color in this figure legend, the reader is referred to the web version of this article) .

Therefore the stability of the photocathode will be determined by the electrochemical resistance of the Pt contact against (photo-) corrosion, which was investigated in a three-electrode photoelectrochemical measurement set-up. Fig. 3(a) presents a galvanostatic stability measurement at a current density of -3 mA/cm^2. The measurement reveals that the photocathode provided a stable potential of around 1.62 V vs. RHE for 50 h of operation. The slow decrease of the potential is attributed to a decreasing level of the electrolyte during the measurement. The two distinct potential steps at 19 h and 43 h of operation, respectively, originate from a refilling of the reservoir in order to cover the whole back contact area of the photocathode with the electrolyte again. In spite of that, the results clearly showed that the Ag/Pt contact effectively protects the a-Si:H/a-Si:H photocathode against electrochemical corrosion and ensures a long-term durability of the photocathode. This result is also confirmed by the cyclic voltammetry measurements, shown in Fig. 3(b), performed before and after the 50 h stability test. It is apparent, that the photocathode performance was not affected by the measurement as both cyclic voltammograms perfectly match. The temperature of the electrolyte slightly changed from 21 °C to 27 °C during the measurement. Related studies however have shown that only temperature differences above 40 °C significantly affect the PV performance, and thus, the PV–EC performance [35].

3.2. Photovoltaic–electrochemical device performance

The solar-to-hydrogen efficiency (η_{STH}) of the PV–EC device based on the adapted a-Si:H/a-Si:H photocathode was evaluated in a two-electrode measurement set-up with a RuO_2 counter electrode (see Fig. 1). Fig. 4 presents the photocurrent density as a

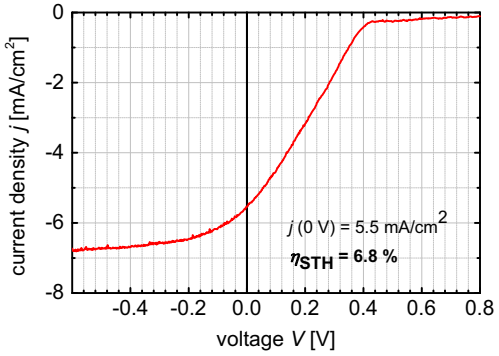

Fig. 4. Linear sweep voltammogram of the a-Si:H/a-Si:H photocathode with Ag/Pt contact in a two-electrode measurement set-up vs. a RuO_2 counter electrode. The measurement was conducted in a 0.1 M H_2SO_4 solution at a scan rate of 30 mV/s.

function of the bias potential, applied between the photocathode and the counter electrode. When the two electrodes were shorted together ($V=0$ V) the measurement revealed that evolution of H_2 occurred at a photocurrent-density of 5.5 mA/cm^2 under simulated sunlight irradiation (100 mW/cm^2). Assuming that the measured photocurrent corresponds to the molecular hydrogen generation via proton reduction (100% faradaic efficiency), the solar-to-hydrogen efficiency of the a-Si:H/a-Si:H device can be determined using the following equation [36]:

$$\eta_{STH} = \frac{\text{power out}}{\text{power in}} = \frac{\Delta E \times j_{op} \times \eta_F}{\text{total integrated power input density}} \quad (1)$$

$\Delta E = 1.23$ V is the thermodynamic potential required for water electrolysis at 25 °C, j_{op} is the operating current when both electrodes are shorted, η_F is the faradaic efficiency for hydrogen evolution, and the input power is the incident light intensity.

The calculation based on Eq. (1) yields an impressive solar-to-hydrogen conversion efficiency of 6.8%, which presents the highest reported STH value for integrated thin film silicon tandem based PV–EC devices. For the given arrangement of the device set-up, using compact and chemically stable electrodes, it can be assumed that the measured photocurrent can be translated into H_2 evolution yield ($\eta_F = 100\%$), even though the generated H_2 and O_2 volumes have not been quantified [37,38]. Faradaic efficiencies of close to 100% are commonly reported for photoelectrodes based on semiconductor structures, including Si and InGaAsP [12,39].

Although, the conversion efficiency is remarkable, the operation point of the PV–EC device does not lie at the maximum power point or in the photocurrent plateau reaching from 6.2 mA/cm^2 to 6.8 mA/cm^2. Thus, the losses in the PV–EC device apparently exceed the 370 mV, mentioned in the beginning of Section 3.1. Nevertheless, this result provides evidence that the amorphous silicon tandem junction PV–EC device concept presented in this study can generate hydrogen without an external bias. A considerably higher solar-to-hydrogen efficiency can be expected by reducing system losses, e.g. by using higher electrolyte concentrations (>0.1 M) or by improving the V_{OC} of the corresponding solar cell, which could shift the operation point of the PV–EC device closer to its maximum power point. The relevant PV–EC loss mechanisms will be analyzed in more detail in the following section.

3.3. Empirical serial circuit model

The two-electrode measurement shown in Fig. 4 displays the overall behavior of the complete PV–EC device. However, this data does not allow to quantitatively evaluate the individual contributions of the PV–EC components separately. To do this, the PV–EC

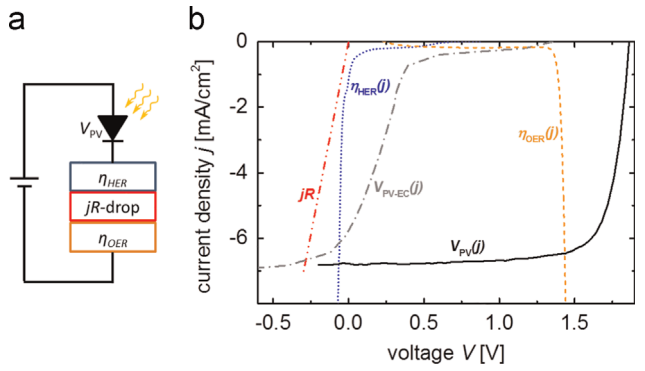

Fig. 5. (a) Simple equivalent circuit of the PV–EC device system, where the four main components are connected in series: the solar cell (V_{PV}), the Pt layer as HER catalyst (η_{HER}), the electrolyte (jR-drop), and the anode for the OER (η_{OER}). (b) Current–voltage and photocurrent–voltage characteristics of the main four circuit components of the PV–EC device: j–V measurement of the a-Si:H/a-Si:H/ZnO:Al/Ag solar cell (V_{PV} (j), black solid curve), j–V measurement of the RuO_2 anode in a 0.1 M H_2SO_4 solution at a scan rate of 10 mV/s (η_{OER} (j), orange dashed curve), j–V measurement of the Pt HER catalyst layer in a 0.1 M H_2SO_4 solution at a scan rate of 10 mV/s (η_{HER} (j), blue dotted curve), and the resistance of the 0.1 M H_2SO_4 electrolyte (jR, red dotted line). The j–V characteristic of the PV–EC device (V_{PV-EC} (j), gray dashed curve) was calculated based on Eq. (2). (For interpretation of the references to color in this figure legend, the reader is referred to the web version of this article).

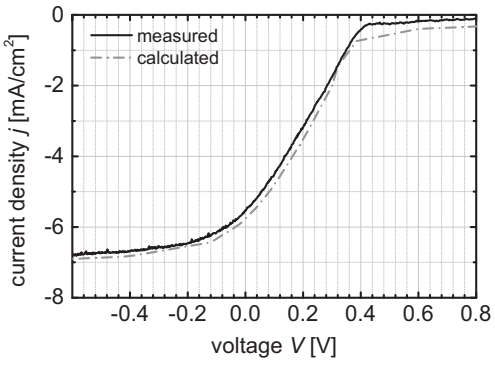

Fig. 6. Comparison of measured (black solid curve, see Fig. 4) and calculated (gray dashed curve) j–V characteristic of the PV–EC device.

device, as depicted in Fig. 1, must be treated as a series connection of its four main circuit components: (1) the a-Si:H/a-Si:H solar cell with the ZnO:Al/Ag back reflector, (2) the thin Pt layer, which was deposited as HER catalyst on top of the ZnO:Al/Ag back reflector, (3) the 0.1 M H_2SO_4 electrolyte, and (4) the RuO_2 anode. Thus, the photocurrent–voltage characteristic V_{PV-EC} (j) of the whole PV–EC device, as measured in a two-electrode set-up, can be calculated via

$$V_{PV-EC}(j) = V_{PV}(j) - \eta_{OER}(-j) + \eta_{HER}(j) + j \cdot R \quad (2)$$

where V_{PV} (j) is the photocurrent–voltage measurement of the a-Si:H/a-Si:H/ZnO:Al/Ag solar cell. η_{OER} (j) is the overpotential for the OER at the RuO_2 anode including the electrode potential for the OER (1.23 V) and η_{HER} (j) is the overpotential for the HER at the Pt layer (measured as Pt electrode alone). Both, η_{OER} (j) and η_{HER} (j) are measured in a three-electrode arrangement. The resistance of the electrolyte is denoted by R. In order to take the different sign of the anodic current for the RuO_2 anode into account, the corresponding three-electrode measurement has to be mirrored at the potential axis, i.e. subtracted in Eq. (2). Fig. 5(a) displays the model underlying series connection of the PV–EC device components. Similar photoelectrochemical device modeling approaches have also been shown elsewhere [40–43].

In fact, as also apparent from Eq. (2), the performance of the PV–EC cell is deteriorated by the relevant loss mechanisms in the system represented by η_{OER} (j), η_{HER} (j), and R: the OER and HER overpotential of the RuO_2 anode and the Pt layer, respectively, and the ohmic drop due to the resistance of the electrolyte given by the value of R (21.3 Ω cm^2, measured by impedance spectroscopy). To graphically illustrate this and draw the comparison between PV and PV–EC characteristics, Fig. 5(b) shows the current–voltage and photocurrent–voltage measurements of the four circuit components given above. The hereout calculated photocurrent–voltage characteristic V_{PV-EC} (j) of the PV–EV device, based on Eq. (2), is also plotted in Fig. 5(b).

This graph allows for a decoupled evaluation of the photoelectrochemical and photovoltaic performance of the complete PV–EC device V_{PV-EC} (j) and of the integrated solar cell V_{PV} (j), respectively and highlights the main differences between both. It is apparent that the saturation photocurrent in both devices is reproduced quantitatively. This was expected because the light absorption and photogeneration and separation of charge carriers in the solar cell remains unaffected in the PV–EC device. The fill factor of the PV–EC device is reduced compared to the PV device, which is mainly due to the additional resistance of the electrolyte. The major difference however occurs in the open-circuit voltage of both devices, which arises from both, the Pt and the RuO_2 electrode overpotential losses as a function of the current. Whereas the a-Si:H/a-Si:H tandem solar cell exhibits a V_{OC} of 1.87 V, the PV–EC shows an calculated onset of cathodic photocurrent at around 1.37 V. This voltage corresponds to a voltage drop of 500 mV, which is higher than the threshold value of 370 mV defined in Section 3.1). This means that for this particular device configuration (Pt and RuO_2 as HER and OER catalysts, respectively) the photovoltage provided by the a-Si:H/a-Si:H solar cell is not sufficient to operate the PV–EC device in its maximum power point and thus, to entirely compensate the overpotential losses.

Fig. 6 presents the comparison between the measured (see Fig. 4) and calculated photocurrent–voltage characteristic of the PV–EC device.

It is apparent, that the calculated j–V curve nearly perfectly matches the experimental data and thus, mirrors the overall behavior of the PV–EC device. This confirms that the presented serial circuit model allows both, the separate evaluation of the losses of the individual PV–EC components, as shown in Fig. 5(b), and the prediction of the overall PV–EC performance considering these losses.

The discrepancy in the region from 0.4 V to 0.8 V, may arise from additional fluctuations in the open circuit potential region during Pt and RuO_2 measurements (see Fig. 5(b)). Additional fluctuations may arise from interfacial charging effects at the Pt-electrolyte and RuO_2-electrolyte double-layer interfaces, respectively [44].

Overall, the presented empirical serial circuit model offers a useful and elegant tool to analyze and predict the performance of integrated PV–EC devices based on experimental data of each individual functional component. Therefore, as the model allows for the decoupled evaluation of all functional device components, one can estimate to what extend an improvement of an individual component (e.g. V_{OC} and J_{SC} of the solar cell or catalytic activity of the HER and OER catalyst material) or a reduction of a specific loss mechanism (e.g. electrolyte resistance or overpotential loss at one of the electrodes) would improve the overall PV–EC device performance and increase STH efficiency further.

4. Conclusions

In conclusion, a direct solar-to-hydrogen conversion efficiency of 6.8% was demonstrated in a two-electrode-arrangement without any

external bias using a photovoltaic–electrochemical device based on an a-Si:H/a-Si:H photocathode with a ZnO:Al/Ag/Pt layer stack contact for the HER and a RuO_2 anode for the OER. Additionally, the a-Si:H/a-Si:H photocathode exhibited a remarkable chemical stability and demonstrated stable performance for over 50 h under operation at -3 mA/cm^2. Based on an empirical serial circuit model, we identified the relevant loss processes in the PV–EC device and could calculate the experimentally measured photocurrent–voltage characteristic of the PV–EC device with high accuracy. The empirical model suggests that further improvements in STH efficiency are feasible when losses are reduced. Nevertheless, our results provide evidence that thin film silicon tandem structures fulfill the main thermodynamic requirements to generate hydrogen under short circuit conditions. The presented PV–EC device concept therefore may offer an alluring approach for related research challenges, including catalyst development [45], robust surface coating designs [46], or integrated device architectures [47] all of which strive for low-cost and efficient devices for solar hydrogen generation.

Acknowledgment

We thank K. Wilken, S. Tillmanns, B. Botar, L. Petter, and A. Lambertz for their contributions to this work. The research is partly financially supported by the Deutsche Forschungsgemeinschaft (DFG) Priority Program 1613 (SPP 1613): Regeneratively produced fuels by light-driven water splitting: Investigation of involved elementary processes and perspectives of technologic implementation, and by the German Bundesministerium für Bildung und Forschung (BMBF) in the network project: Sustainable Hydrogen (FKZ 03X3581A and FKZ 03X3581B). J. Ziegler, B. Kaiser, and W. Jaegermann acknowledge partial financial support by the DFG Excellence Graduate School of Energy Science and Engineering (GSC 1070).

References

[1] C.A. Grimes, O.K. Varghese, S. Ranjan, Light, Water, Hydrogen: The Solar Generation of Hydrogen by Water Photoelectrolysis, Springer, New York, 2008.
[2] J.R. McKone, N.S. Lewis, H.B. Gray, Will solar-driven water-splitting devices see the light of day? Chem. Mater. 26 (2014) 407–414.
[3] N.S. Lewis, D.G. Nocera, Powering the planet: chemical challenges in solar energy utilization, Proc. Natl. Acad. Sci. USA 103 (2006) 15729–15735.
[4] E. Miller, White papers on materials for photoelectrochemical water splitting, DOE PEC Working Group, 2013. Available at ⟨http://energy.gov/eere/fuelcells/downloads/white-papers-materials-photoelectrochemical-water-splitting⟩.
[5] A. Fujishima, K. Honda, Electrochemical photolysis of water at a semiconductor electrode, Nature 238 (1972) 37–38.
[6] A.J. Nozik, J. Miller, Introduction to solar photon conversion, Chem. Rev. 110 (2010) 6443–6936.
[7] L.J. Minggu, W.R. Wan Daud, M.B. Kassim, An overview of photocells and photoreactors for photoelectrochemical water splitting, Int. J. Hydrog. Energy 35 (2010) 5233–5244.
[8] R. Van de Krol, M. Grätzel, Photoelectrochemical Hydrogen Production, Springer, New York, 2012.
[9] B. Seger, D.S. Tilley, T. Pedersen, P.C.K. Vesborg, O. Hansen, M. Grätzel, I. Chorkendorff, Silicon protected with atomic layer deposited TiO_2: durability studies of photocathodic H_2 evolution, RSC Adv. 3 (2013) 25902–25907.
[10] E. Aharon-Shalom, A. Heller, Efficient p - InP (Rh - H alloy) and p - InP (Re - H alloy) hydrogen evolving photocathodes, J. Electrochem. Soc. 129 (1982) 2865–2866.
[11] M. Malizia, B. Seger, I. Chorkendorff, P.C.K. Vesborg, Formation of a p–n heterojunction on GaP photocathodes for H_2 production providing an open-circuit voltage of 710 mV, J. Mater. Chem. A 2 (2014) 6847–6853.
[12] O. Khaselev, J.A. Turner, A monolithic photovoltaic–photoelectrochemical device for hydrogen production via water splitting, Science 280 (1998) 425–427.
[13] K. Sun, S. Shen, Y. Liang, P.E. Burrows, S.S. Mao, D. Wang, Enabling silicon for solar-fuel production, Chem. Rev. 114 (2014) 8662–8719.
[14] B. Seger, A.B. Laursen, P.C.K. Vesborg, T. Pedersen, O. Hansen, S. Dahl, I. Chorkendorff, Hydrogen production using a molybdenum sulfide catalyst on a titanium-protected n^+p-silicon photocathode, Angew. Chem. Int. Ed. 51 (2012) 9128–9131.
[15] R.N. Dominey, N.S. Lewis, J.A. Bruce, D.C. Bookbinder, M.S. Wrighton, Improvement of photoelectrochemical hydrogen generation by surface modification of p-type silicon semiconductor photocathodes, J. Am. Chem. Soc. 104 (1982) 467–482.
[16] H. Tributsch, Layer-type transition metal dichalcogenides—a new class of electrodes for electrochemical solar cells, Ber. Bunsenges. phys. Chem. 81 (1977) 361–369.
[17] H. Tributsch, Hole reactions from d-energy bands of layer type group VI transition metal dichalcogenides: new perspectives for electrochemical solar energy conversion, J. Electrochem. Soc. 125 (1978) 1086–1093.
[18] G. Kline, K.K. Kam, R. Ziegler, B.A. Parkinson, Further studies of the photoelectrochemical properties of the group VI transition metal dichalcogenides, Sol. Energy Mater. 6 (1982) 337–350.
[19] J.R. McKone, A.P. Pieterick, H.B. Gray, N.S. Lewis, Hydrogen evolution from Pt/Ru-coated *p*-Type WSe_2 photocathodes, J. Am. Chem. Soc. 135 (2013) 223–231.
[20] T.J. Jacobsson, V. Fjällström, M. Sahlberg, M. Edoff, T. Edvinsson, A monolithic device for solar water splitting based on series interconnected thin film absorbers reaching over 10% solar-to-hydrogen efficiency, Energy Environ. Sci. 6 (2013) 3676–3683.
[21] K. Sivula, F. Le Formal, M. Grätzel, Solar water splitting: progress using hematite (α-Fe_2O_3) photoelectrodes, ChemSusChem 4 (2011) 432–449.
[22] J. Gan, X. Lu, Y. Tong, Towards highly efficient photoanodes: boosting sunlight-driven semiconductor nanomaterials for water oxidation, Nanoscale 6 (2014) 7142–7164.
[23] F.F. Abdi, L. Han, A.H.M. Smets, M. Zeman, B. Dam, R. van de Krol, Efficient solar water splitting by enhanced charge separation in a bismuth vanadate-silicon tandem photoelectrode, Nat. Commun. 4 (2013) 2195.
[24] S. Hu, C. Xiang, S. Haussener, A.D. Berger, N.S. Lewis, An analysis of the optimal band gaps of light absorbers in integrated tandem photoelectrochemical water-splitting systems, Energy Environ. Sci. 6 (2013) 2984–2993.
[25] J.R. Bolton, S.J. Strickler, J.S. Connolly, Limiting and realizable efficiencies of solar photolysis of water, Nature 316 (1985) 495–500.
[26] M.F. Weber, M.J. Dignam, Efficiency of splitting water with semiconducting photoelectrodes, J. Electrochem. Soc. 31 (1984) 1258–1265.
[27] S. Licht, B. Wang, S. Mukerji, T. Soga, M. Umeno, H. Tributsch, Over 18% solar energy conversion to generation of hydrogen fuel; theory and experiment for efficient solar water splitting, Int. J. Hydrog. Energy 26 (2001) 653–659.
[28] S.Y. Reece, J.A. Hamel, K. Sung, T.D. Jarvi, A.J. Esswein, J.J.H. Pijpers, D.G. Nocera, Wireless solar water splitting using silicon-based semiconductors and earth-abundant catalysts, Science 334 (2011) 645–648.
[29] L. Han, F.F. Abdi, P. Perez Rodriguez, B. Dam, R. van de Krol, M. Zeman, A.H.M. Smets, Optimization of amorphous silicon double junction solar cells for an efficient photoelectrochemical water splitting device based on a bismuth vanadate photoanode, Phys. Chem. Chem. Phys. 16 (2014) 4220–4229.
[30] E.L. Miller, R.E. Rocheleau, S. Khan, A hybrid multijunction photoelectrode for hydrogen production fabricated with amorphous silicon/germanium and iron oxide thin films, Int. J. Hydrog. Energy 29 (2014) 907–914.
[31] A. Shah, Thin-Film Silicon Solar Cells, Photovoltaics and Large-area Electronics, EPFL Press, Switzerland, 2008.
[32] F. Urbain, K. Wilken, V. Smirnov, O. Astakhov, A. Lambertz, J.-P. Becker, U. Rau, J. Ziegler, B. Kaiser, W. Jaegermann, F. Finger, Development of thin film amorphous silicon tandem junction based photocathodes providing high open-circuit voltages for hydrogen production, Int. J. Photoenergy 2014 (2014) 249317.
[33] W. Böttler, V. Smirnov, J. Hüpkes, F. Finger, Texture-etched ZnO as a versatile base for optical back reflectors with well-designed surface morphologies for application in thin film solar cells, Phys. Status Solidi A 209 (2012) 1144–1149.
[34] G. Hodes, Photoelectrochemical cell measurements: getting the basics right, J. Phys. Chem. Lett. 3 (2012) 1208–1213.
[35] M. Shima, M. Isomura, K.-I. Wakisaka, K. Murata, M. Tanaka, The influence of operation temperature on the output properties of amorphous silicon-related solar cells, Sol. Energy Mater. Sol. Cells 85 (2005) 167–175.
[36] Z. Chen, T.F. Jaramillo, T.G. Deutsch, A. Kleiman-Shwarsctein, A.J. Forman, N. Gaillard, R. Garland, K. Takanabe, K. Heske, M. Sunkara, E.W. McFarland, K. Domen, E. Miller, J.A. Turner, H.N. Dinh, Accelerating materials development for photoelectrochemical hydrogen production: standards for methods, definitions, and reporting protocols, J. Mater. Res. 25 (2010) 3–16.
[37] M.G. Walter, E.L. Warren, J.R. McKone, S.W. Boettcher, Q. Mi, E.A. Santori, N.S. Lewis, Solar water splitting cells, Chem. Rev. 110 (2010) 6446–6473.
[38] Z. Chen, H.N. Dinh, E. Miller, Photoelectrochemical Water Splitting, Springer, New York, 2013.
[39] D.V. Esposito, I. Levin, T.P. Moffat, A.A. Talin, H_2 evolution at Si-based metal-insulator-semiconductor photoelectrodes enhanced by inversion channel charge collection and H spillover, Nat. Mater. 12 (2013) 562–568.
[40] M.T. Winkler, C.R. Cox, D.G. Nocera, T. Buonassisi, Modeling integrated photovoltaic–electrochemical devices using steady-state equivalent circuits, Proc. Natl. Acad. Sci. USA 110 (2012) 1076–1082.
[41] T.J. Mills, F. Lin, S.W. Boettcher, Theory and simulations of electrocatalyst-coated semiconductor electrodes for solar water splitting, Phys. Rev. Lett. 112 (2014) 148304.
[42] Z. Huang, J.R. McKone, C. Xiang, R.L. Grimm, E.L. Warren, J.M. Spurgeon, H.-J. Lewerenz, B.S. Brunschwig, N.S. Lewis, Comparison between the measured and modeled hydrogen-evolution activity of Ni- or Pt-coated silicon photocathodes, Int. J. Hydrog. Energy 39 (2014) 16220–16226.
[43] J. Ziegler, B. Kaiser, W. Jaegermann, F. Urbain, J.-P. Becker, V. Smirnov, F. Finger, Photoelectrochemical and photovoltaic characteristics of amorphous-silicon-

based tandem cells as photocathodes for water splitting, ChemPhysChem 15 (2014) 4026–4031.
[44] A.J. Bard, L.R. Faulkner, Electrochemical Methods: Fundamentals and Applications, second ed., John Wiley & Sons, New York, 2001.
[45] K. Maeda, K. Domen, Photocatalytic water splitting: recent progress and future challenges, J. Phys. Chem. Lett. 1 (2010) 2655–2661.
[46] B. Mei, B. Seger, T. Pedersen, M. Malizia, O. Hansen, I. Chorkendorff, P.C.K. Vesborg, Protection of p^+-n-Si Photoanodes by Sputter-Deposited Ir/IrO_x Thin Films, J. Phys. Chem. Lett. 5 (2014) 1948–1952.
[47] B. Seger, I.E. Castelli, P.C.K. Vesborg, K.W. Jacobsen, O. Hansen, I. Chorkendorff, 2-Photon tandem device for water splitting: comparing photocathode first versus photoanode first designs, Energy Environ. Sci. 7 (2014) 2397–2413.